

Shear-Induced Precursor Relaxation-Dependent Growth Dynamics and Lamellar Orientation of β -Crystals in β -Nucleated Isotactic Polypropylene

Yan-Hui Chen,^{†,‡} Du-Fei Fang,[§] Jun Lei,[‡] Liang-Bin Li,^{||} Benjamin S. Hsiao,[§] and Zhong-Ming Li^{*,‡}

[†]Department of Applied Chemistry, School of Science, Northwestern Polytechnical University, Xi'an 710129, China

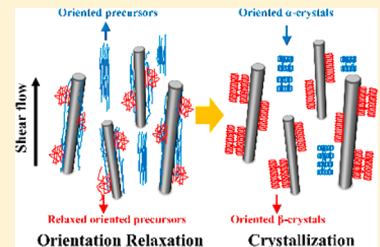
[‡]College of Polymer Science and Engineering and State Key Laboratory of Polymer Materials Engineering, Sichuan University, Chengdu 610065, China

[§]Department of Chemistry, Stony Brook University, Stony Brook, New York 11794-3400, United States

^{||}National Synchrotron Radiation Lab and College of Nuclear Science and Technology, CAS Key Laboratory of Soft Matter Chemistry, University of Science and Technology of China, Hefei 230022, China

S Supporting Information

ABSTRACT: Although a shear flow field and β -nucleating agents (β -NAs) can separately induce the formation of β -crystals in isotactic polypropylene (iPP) in an efficient manner, we previously encountered difficulty in obtaining abundant β -crystals when these two factors were applied due to the competitive growth of α - and β -crystals. In the current study, to induce the formation of a high fraction of β -crystals, a strategy that introduces a relaxation process after applying a shear flow field but before cooling to crystallize β -nucleated iPP was proposed. Depending on the relaxation state of the shear-induced oriented precursors, abundant β -crystals with a refined orientation morphology were indeed formed. The key to producing these crystals lay in the partially dissolved shear-induced oriented precursors as a result of the relaxation process's ability to generate β -crystals by inducing the formation of needlelike β -NAs. Therefore, the content of β -crystals gradually increased with relaxation time, whereas the overall crystallization kinetics progressively decreased. Moreover, more time was required for the content of the β -phase to increase to the (maximum) value observed in quiescent crystallization than for the effect of flow on crystallization kinetics to be completely eliminated. The *c*-axis of the oriented β -lamellae was observed to be perpendicular, rather than parallel, to the fiber axis of the needlelike β -NAs, as first evidenced by the unique small-angle X-ray scattering patterns obtained. The significance of the relaxation process was manifested in regulating the content and morphology of oriented β -crystals in sheared, β -nucleated iPP and thus in the structure and property manipulation of iPP.



1. INTRODUCTION

The β -polymorph of isotactic polypropylene (iPP) has long been of interest to the polymer research community due to its unique crystallographic characteristics and profound influences on mechanical performances. Its complex, geometrically frustrated structure makes β -phase the last unresolved aspect concerning the polymorphism of iPP (as far as our current understanding is concerned).¹ From an application point of view, β -phase can be utilized to control iPP-related materials' toughness by means of two routines. On one hand, the loose chain packing style of β -phase itself results in better toughness and ductility.^{2–5} Moreover, the fraction of β -phase with regard to the common α -phase content can be controlled by fine-tuning processing parameters, such as temperature, due to its metastable nature.^{6,7} On the other hand, the morphology of β -phase plays a key role in tuning the toughness of iPP.^{8,9} Due to sufficient connections between the crystallites, β -“flower”-like agglomerate crystallites were reported to demonstrate the largest strain at break (the best ductility) compared to other crystal morphologies, such as β -spherulites and β -transcrystalline entities.⁹

Unfortunately, toughness is usually improved at the expense of strength. It is challenging to achieve simultaneous reinforcement and toughening of iPP.⁴ As far as strength is considered, oriented crystal structures, such as shish-kebabs consisting of a central fibril polymer chain bundle (shish) and lamellar crystal attached to it (kebab), are able to significantly enhance the material's modulus and strength.^{10,11} Following this reasoning, it is hypothesized that the strength of β -phase-rich iPP can also be improved by inducing highly oriented β -crystals. However, owing to thermodynamic and mechanical instability, β -phase crystal is difficult to orient under external forces; instead, it tends to transform into α -phase (or mesomorphic phase under various circumstances).^{12–14} Other attempts, such as applying shear flow to the iPP sample with β -nucleating agents (β -NAs), also resulted in failure, where the β -crystals are greatly depressed without evidence of orientation.^{4,15} There are, nevertheless, several successful practices. For instance, by

Received: February 12, 2015

Revised: March 31, 2015

Published: April 3, 2015

pulling fibers in an iPP melt,¹⁶ mixing iPP fibers in a molten or partially molten state into an isotropic iPP melt,¹⁷ or annealing an oriented iPP melt with the aid of a temperature gradient,¹⁸ a limited amount of β -phase with a preferred orientation can be achieved. Surprisingly, applying a shear flow and adding β -NAs is later demonstrated as a feasible method that can realize the orientation of β -crystals in practice,^{19–22} although this finding appears counterintuitive.^{4,15} Yamaguchi et al. conducted a detailed analysis of the orientation mode of β -crystals induced by β -NAs in the injection-molded or extruded iPP using a wide-angle X-ray scattering technique.^{19–22} They carefully compared diffraction patterns in three orthogonal directions, namely, the machine direction (MD), the normal direction (ND), and the transverse direction (TD). An anomalous β -crystal orientation mode with its *c* axis perpendicular to the flow direction, due to the epitaxial growth habit of β -crystals on the β -NAs' surface, was revealed. This unique feature explains various facts of injection-molded iPP products: oriented β -crystals in iPP sheets impart the mechanical anisotropy. For example, ductile behavior occurs in the TD, whereas the material is brittle along the MD.

To determine the orientation of β -crystals under real processing conditions, we must decouple the roles of β -NAs and flow. The effectiveness of β -NAs is purely because of the epitaxial crystal growth habit of β -phase.²³ The influence of flow is two-fold: flow can not only orient nonspherical β -NAs²⁴ but also effectively orient polymer molecular chains, which thereby induces stable α -phase.⁵ With the presence of both β -NA and flow, there exist two competitive processes (i.e., the growth of α - and β -phase), as previously observed by our group; details can be found elsewhere.^{4,15} It should be noted that the competitive growth of α - and β -phase is kinetically-controlled. The lifetime of oriented polymer molecular chain segments (i.e., shear-induced oriented precursors) is highly temperature-dependent.²⁵ Once relaxed, the growth of β -phase is favorable in the presence of β -NAs. Thus, relaxation of oriented polymer molecular chains is the key to manipulating the oriented β -crystals, which has not yet been addressed.

In this work, the effect of the relaxation of oriented polymer molecular chains on the formation of oriented β -crystals in sheared β -nucleated iPP was fully addressed by using an *in situ* X-ray scattering technique. It was determined that regulating the relaxation degree of shear-induced oriented precursors was beneficial to achieving the optimal content and orientation of β -crystals. Our study provides a new strategy to manipulate the crystal forms in the sheared β -nucleated iPP and, further, the structure and properties of the iPP.

2. EXPERIMENTAL SECTION

2.1. Materials. iPP was purchased from Dushanzi Petroleum Chemical Company, Xinjiang, China. The molecular weight $M_w = 39.9 \times 10^4$ g mol⁻¹, and the polydispersity $M_w/M_n = 4.6$. The melt flow rate was 3 g/10 min (230 °C, 21.6 N). Aryl amide compound (TMB-5) was used as β -NA; its chemical structure is similar to some aromatic amine β -NAs, such as *N* and *N'*-dicyclohexyl-2,6-naphthalenedicarboxamide. This compound was kindly provided by Fine Chemical Institute of Shanxi, Taiyuan, China.

2.2. Sample Preparation. β -NAs were melt mixed with iPP using a twin-screw extruder. The concentration of β -NAs was 0.05 wt %. The screw speed was 82 rpm, and the processing temperature window was set between 170 to 180 °C from hopper to die. The extruded pellets were then compressed

into films with a thickness of 0.5 mm at 200 °C for 5 min, and then air-cooled down to room temperature.

2.3. In Situ WAXD/SAXS Measurements. Wide-angle X-ray diffraction (WAXD) and small-angle X-ray scattering (SAXS) measurements were carried out at the Advanced Polymers Beamline (X27C) in the National Synchrotron Light Source (NSLS), Brookhaven National Laboratory (BNL). The wavelength of the X-rays was $\lambda = 0.1371$ nm. A MAR CCD (1024 × 1024 pixels, pixel size = 158.4 μm) was employed to record 2D-WAXD/SAXS images. The data acquisition time was 20 s for each scattering image. The sample-to-detector distance (SSD) was 112.9 mm for WAXD (calibrated by aluminum oxide) and 1844 mm for SAXS (calibrated by silver behenate).

A Linkam CSS-450 high-temperature shearing stage modified for *in situ* X-ray scattering studies was used to control precisely the shear flow and thermal history of the polymer samples. The temperature and shear conditions used in the WAXD and SAXS measurements are shown in Figure 1. Details of the

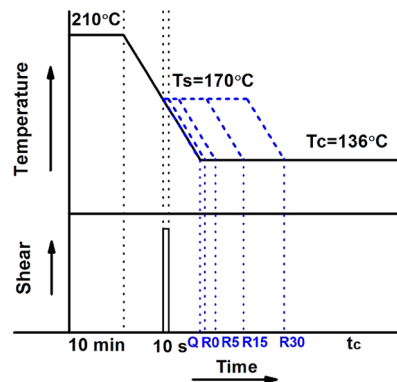


Figure 1. Schematic of the temperature and shear conditions applied (step shear of 30 s⁻¹ for 10 s) as a function of time for WAXD and SAXS experiments.

experimental protocol are as follows: (1) heat the sample quickly from room temperature to 210 °C, with a heating rate of 100 °C/min; (2) hold at 210 °C for 10 min to eliminate any residual structure; (3) cool to 170 °C at 30 °C/min, and apply a step shear (the shear rate was 30 s⁻¹ with the duration of 10 s) when reaching this temperature; (4) after the shear, hold the temperature at 170 °C for different time intervals, namely, 0, 5, 15, and 30 min, to relax the sample. The samples relaxed for different times are denoted as R0, R5, and R15; (5) cool to 136 °C at 30 °C/min; and (6) crystallize the sample at 136 °C. The isothermal crystallization process at 136 °C was monitored using *in situ* WAXD or SAXS, as described before. For comparison purposes, quiescent isothermal crystallization (without step shear and stopping at 170 °C, denoted Q) was utilized.

1D scattering profiles were obtained from the circular average of 2D-WAXD/SAXS patterns, where scattering intensity was plotted as a function of the modulus of the reciprocal space vector, s ($|s| = 2 \sin \theta / \lambda$, with λ being the wavelength of the incident beam and 2θ being the scattering angle). In 1D-SAXS profiles, the long period (L_B) that defines the statistical average of the distance between two lamellar crystals is related to the position of the first intensity maximum (s_m) by $L_B = 1/s_m$. For 1D-WAXD profiles, the crystallinity index X_c was calculated using eq 1.

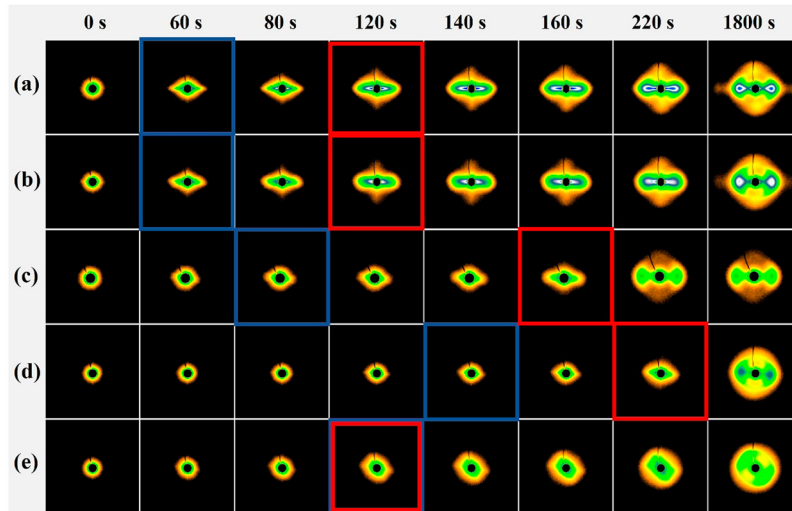


Figure 2. Selected 2D-SAXS patterns showing the lamellar growth of iPP with 0.05% β -NAs isothermally crystallized at 136 °C. (a) relax 0 min after the shear (R0), (b) relax 5 min after the shear (R5), (c) relax 15 min after the shear (R15), and (d) relax 30 min after the shear (R30) prior to isothermal crystallization and (e) quiescent isothermal crystallization without shear (Q). The shear direction is vertical. The blue and red rectangles denote the initial appearance of the TD and MD scattering signals, respectively.

$$X_c = \frac{\sum A_{\text{cryst}}}{\sum A_{\text{cryst}} + \sum A_{\text{amorp}}} \quad (1)$$

where A_{cryst} and A_{amorp} are areas of diffraction peaks from crystals and diffused scattering from the amorphous matrix, respectively. Following Turner-Jones,²⁶ when the system consists of both α - and β -phase, the relative content of the β -crystals (K_β) can be evaluated using the ratio of the area of β -phase's signature diffraction peak over the total area of major diffraction peaks, given in eq 2

$$K_\beta = \frac{A_\beta(110)}{A_\beta(110) + A_\alpha(110) + A_\alpha(040) + A_\alpha(130)} \quad (2)$$

In eq 2, $A_\beta(110)$ represents the area of the diffraction peak of (110) for β -phase; $A_\alpha(110)$, $A_\alpha(040)$, and $A_\alpha(130)$ represent that of signature diffraction peaks, namely, (110), (040), and (130), of α -phase. The crystallinity index of β -crystals (X_β) in this case is given by

$$X_\beta = K_\beta X_c \quad (3)$$

Historically, the signature diffraction peak of the β -phase was designated as (300) for a hexagonal unit cell.²⁶ It turned out to be the (110) plane in a trigonal unit cell, which is the correct crystal structure (see Figure S1 of the Supporting Information).²⁷

2.4. Polarized Light Microscopy (PLM). Direct morphological observation of β -crystal growth on the β -NAs was performed using an Olympus BX-51 polarized light microscopy (PLM) (with a tilting compensator) combined with a CSS-450 high-temperature shearing stage. The sample (30 μm thick) was first heated to 210 °C with a heating rate of 30 °C/min and was kept at this temperature for 10 min to eliminate thermal history. Subsequently, the molten film was cooled down to 170 °C; a step shear with a shear rate of 30 s^{-1} was then applied for 10 s. After the cessation of the shear, the sample was immediately cooled down to 136 °C at a rate of 30 °C/min. The sample was held at 136 °C for 30 min to allow the completion of the isothermal crystallization process. PLA micrographs were captured every 30 s during annealing.

3. RESULTS AND DISCUSSION

3.1. Orientation and Evolution of β -Lamellae. To elucidate the lamellar periodicity,^{28,29} SAXS patterns of iPP samples during isothermal crystallization after being relaxed at 170 °C for different amounts of time are shown in Figure 2, where the flow direction (or the machine direction, MD) is vertical; the horizontal direction is defined as the transverse direction (TD). After application of the step shear, sample R0 (without any relaxation duration at 170 °C) starts to exhibit weak streaks along the TD at approximately 60 s followed by emergence of intensity maxima along the MD at approximately 120 s. In the late stage of crystallization (say, 1800 s), a crosslike scattering pattern showing intensity maxima along both the MD and TD was observed (Figure 2a). Furthermore, high-order scattering maxima appeared along the TD.^{30,31}

Considering the complex nature of our system (i.e., the coexistence of both β -NAs and shear flow), we need to carefully sort out several features in Figure 2. The intensity maxima along the MD should be mainly caused by α -lamellae,^{32,33} with its development consistent with evolution of α -crystal signature diffraction peaks in WAXD patterns (see Figure 6a, for example). The streaks along the TD in the early stage were normally supposed to have a shish-like structure consisting of oriented polymer chain bundles.^{25,33–35} In principle, needlelike particles, such as β -NAs, can also cause scattering streaks. If this is the case, the streaks should exist at the start (before the appearance of crystal diffraction in WAXD patterns),²⁵ which is not true in our experiment (see Figure 6a). In addition, the concentration of β -NAs (0.05 wt %) is too low to produce noticeable scattering signals.

Shear-induced crystallization of iPP has been well-studied.^{36–38} Normally, the streaks along the TD were reported to appear before occurrence of lobes along the MD in SAXS experiments, due to the generation of shear-induced crystallization precursors.^{25,33–35} This appeared to be the case in our experiments, as shown in Figure 2a. However, a difference arose when the TD intensity continued to increase, and intensity maxima formed, indicating the existence of a well-oriented layered structure rather than its decay or disappearance, which

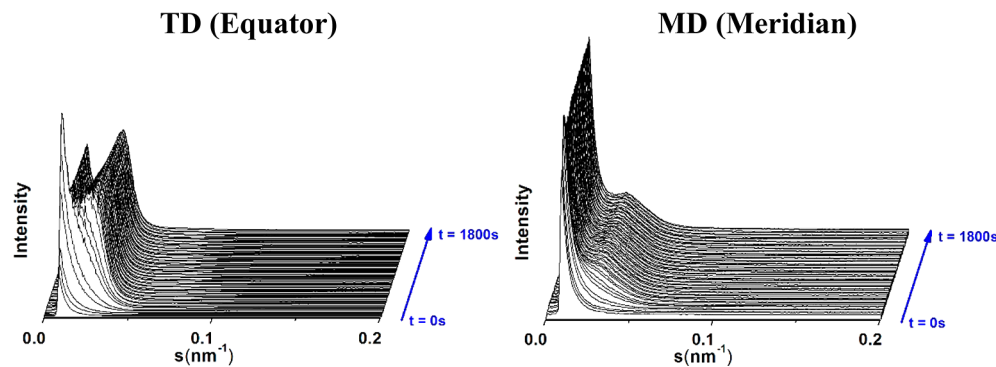


Figure 3. SAXS profiles (linear scale) of sheared iPP with 0.05 wt % β -NAs without relaxation (sample R0). 1D profiles were obtained by averaging a fanlike region centered at MD (right) and TD (left), with an azimuthal spread angle of 90 deg (± 45 deg around MD or TD).

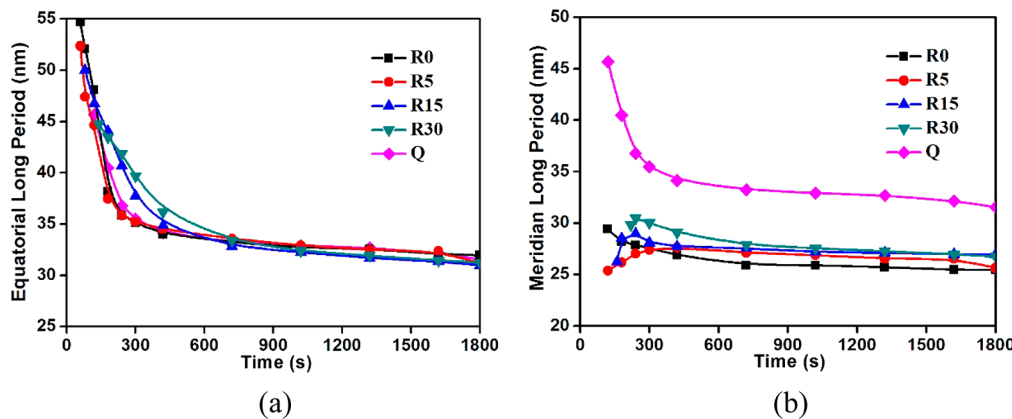


Figure 4. Time evolution profiles of the long periods as a function of crystallization time at (a) TD and (b) MD.

is normally observed for unstable shish-like structures.³⁹ Combining with WAXD data (Figure 6a), we notice that the strengthening of the TD intensity in SAXS patterns is in pace with the occurrence of β -crystal in WAXD patterns. Because β -phase is mainly induced by β -NAs via epitaxial growth, the orientation of needlelike β -NA particles becomes critical in interpreting the TD intensity maxima in SAXS patterns. It needs to be noted that shear flow is actually complex in nature: it features a uniaxial extension component and a rotation component.⁴⁰ For rigid anisotropic particles subjected to shear flow, the rotation component is able to generate tumbling motion. Consequently, both a parallel orientation with the long-axis of the particles parallel to the MD and a perpendicular orientation with the long-axis orthogonal to the MD can be developed, depending on various experimental conditions, such as matrix viscosity, shear rate, and strain. For the constrained shear experiments carried out by the shear stage, such as ours, the perpendicular orientation mode is essentially impossible to develop due to the limited space.^{41,42} It is quite odd that the parallel orientation of β -NAs with β -lamellae grown upon their surface gives rise to the TD intensity maxima, if it follows the template effect of carbon nanotubes inducing perpendicular lamellae.⁴¹ The only rational explanation is that the β -lamellae grow parallel instead of perpendicular to the long-axis of β -NAs. In other words, the *c* axis of the β -lamellae is perpendicular to the long-axis of β -NAs. This finding is the first verification of the anomalous β -lamellae using the SAXS technique. This phenomenon will be further discussed based on PLM images (Figure 5) and WAXD data (Figure 6).

For the samples crystallizing after being relaxed for different amounts of time (5, 15, and 30 min) shown in Figure 2 (panels b-d), the prolonged relaxation time renders the samples a delayed appearance of the TD streaks, along with the successive presence of the MD maxima, as a consequence of the decay of shear-induced oriented precursors. Additionally, the MD intensity at 1800 s decreases as the time allowed for the sample to relax increases. This is reasonable because high temperature annealing tends to melt away shear-induced oriented precursors, causing the growth of α -lamellae to be less favorable. At this high relaxation temperature, the viscosity of the polymer matrix is lower; this makes it difficult for β -NA to maintain its original orientation state. Therefore, not only do the TD intensity maxima become weaker, but the circular intensity distribution also becomes broader. Figure 2e shows SAXS patterns obtained during isothermal crystallization of the quiescent sample (without being sheared, i.e., sample Q), for comparison purposes. In this case, the entire scattering patterns are mainly derived from β -lamellae, which can also be evidenced from WAXD data in Figure 6e. Due to the external forces introduced during sample preparation (i.e., compression), β -NAs were preferentially distributed in their initial state, upon which β -lamellae contribute to the anisotropic SAXS patterns.

To differentiate development of α - and β -phase lamellar structures, we integrated separate intensity near the MD and TD (± 45 deg in the vicinity of the MD or TD). A typical waterfall plot of 1D scattering profile evolution along the MD and TD during isothermal crystallization of the sample R0 is shown in Figure 3, corresponding to the SAXS patterns shown

in Figure 2a. Similar plots of samples R5, R15, R30, and Q are all included in the Supporting Information for simplification (Figure S2 of the Supporting Information). From 1D profiles, the so-called long period (L_B) along the MD and TD can be derived, given that both of the MD and TD profiles show an intensity maximum. Changes of a long period as a function of crystallization time are shown in Figure 4. In Figure 4a, all the TD long periods start from a maximum value, subsequently decrease markedly and eventually level off at a constant value, as a result of the progression of crystallization. With increasing the relaxation time from 0 to 30 min, the initial TD long periods become shorter, and the time required to achieve the same plateau equilibrium is prolonged, as evidenced by the slowly flattened curves. Although they could not be detected by SAXS, certain ordered structures in the partially relaxed shear-induced oriented precursors continued to accumulate with the elapse of crystallization time. Once its size overpasses the SAXS detection percolation threshold, the scattering lamellar maximum appears and the long period can be obtained, but exhibiting a decreasing initial value dependent on the relaxation time. It is understandable that the decay of shear-induced oriented precursors not only causes a postponed SAXS signal (Figure 2, panels b–d) but also slows down the evolution of lamellae. In Figure 4b, the MD long periods of samples Q and R0 present an analogous variation to the TD long periods. However, the MD long periods of the relaxed samples (R5, R15, and R30) demonstrate a mild rise before a slight drop to a constant value. A moderate growth of the MD long periods is observed with the increase of the relaxation time in the entire crystallization process, except for a few points in the early stage of sample R5. The long periods are correlated with the stacking manner of polymer molecular chains,¹⁵ specifically, α or β -lamellae in our case. Corresponding to the loose β -lamellae whose lamellae often diverge from the initial lamellar arrangement,^{43–45} it is fair to see that the resultant long periods in the TD are roughly 6.5 nm larger than that in the MD. It is conceivable that the presence of some β -lamellae in the MD contributes to the augment of the MD long periods in the relaxed samples due to the favorable temperature for epitaxial growth of β -lamellae.¹⁶

As a supplementary characterization for the orientation of β -lamellae and solid verification of the work carried out by Yamaguchi et al.,¹⁹ macroscopic morphological observation was performed on sample R0 by PLM, as shown in Figure 5. Abundant needlelike β -NA crystals set in before the application of the shear flow field (not shown here). Right after the shear flow, needlelike β -NA crystals have developed to approximately 5 μm in diameter and 50 μm in length, and most are oriented along the shear flow direction (Figure 5a), displaying a yellow long axis (Figure 5b). The gradually growing β -crystals exhibit the same color as the needlelike β -NAs do (Figure 5, panels c and d). This phenomenon unequivocally manifests as the arrangement of the c -axis of the β -crystals perpendicular to the long-axis of the needlelike β -NAs crystals, which is basically in line with what was observed by Yamaguchi et al.¹⁹ It needs to be stressed here that the shear flow field and needlelike β -NA crystals aligning along the shear flow field direction are two essential elements to generate these anomalous oriented β -crystals. Without either of them, oriented β -crystals will fail to form. Reminiscent of β -lamellae in sample Q (Figure 2e), its random preferential direction is exactly ascribed to the absence of a strong shear flow field. Otherwise, the formation of needlelike β -NA crystals primarily depends on the critical

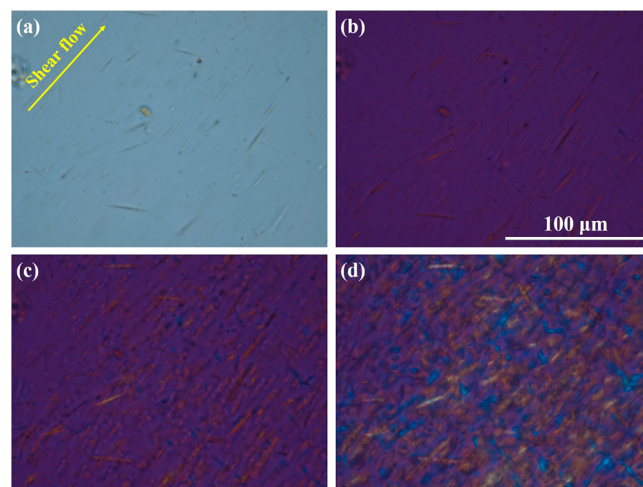


Figure 5. PLM photographs of quiescently isothermal crystallization of iPP with 0.05 wt % β -NAs after the step shear at 136 °C. (a) 0 s with parallel analyzer; (b) 0 s; (c) 450 s; and (d) 900 s.

temperature and concentration, to which attention must be paid.^{9,46}

3.2. Crystallization of Oriented β -Crystals after Relaxation. To explore the effect of relaxation on the crystallization of oriented β -crystals, in situ WAXD measurement was performed. Figure 6 displays selected 2D-WAXD images during the isothermal crystallization process of β -nucleated iPP samples at 136 °C. Experimental conditions are similar to those shown in Figure 2, namely, different relaxation durations (0, 5, 15, and 30 min, using the same notations) at 170 °C were allowed before decreasing to 136 °C to crystallize the sheared samples. Crystallization of a β -nucleated sample without being sheared is also shown (sample Q in Figure 6e) for comparison purposes, where a series of isotropic Debye–Scherrer rings are observed as iPP crystals are randomly dispersed. Under this quiescent condition, due to the high-efficiency β -nucleation effect of β -NAs, it is understandable that β -phase is dominant, as evidenced by the strong signature diffraction peak $\beta(110)$. Much clearer diffraction peaks can be observed from the 1D diffraction profiles in Figure 7e.

It has been well-documented that shear flow is able to induce the crystallization precursors consisting of aligned chain segments, which is favorable for the initial growth of α -crystals in iPP.^{25,32} As observed in sample R0, α -crystals start growing at the very beginning of isothermal crystallization (at roughly 0 s), while the presence of β -crystals first occurs at roughly 80 s (Figures 6a and 7a). The enhanced α -crystals' growth readily restricts the competitive growth of β -crystals induced by β -NAs. The resulting content of β -crystals is significantly lowered because of the more favorable condition for α -crystal growth provided by shear flow. This phenomenon has been elaborately analyzed in our previous work, which revealed the unexpected competitive growth of α - and β -nuclei in iPP when shear flow and β -NAs coexisted where the relaxation process was not introduced before crystallization.¹⁵

As the relaxation time increases (R5 and R15), crystallization of α -crystals slows down, while β -crystals' growth is greatly enhanced. As seen in Figure 6 (panels b and c) and Figure 7 (panels b and c), the induction period of the α -phase crystal is prolonged to approximately 20 s, while β -crystals start to occur at an earlier time, namely, approximately 60 s. Increasing relaxation time at the high temperature allows shear-induced

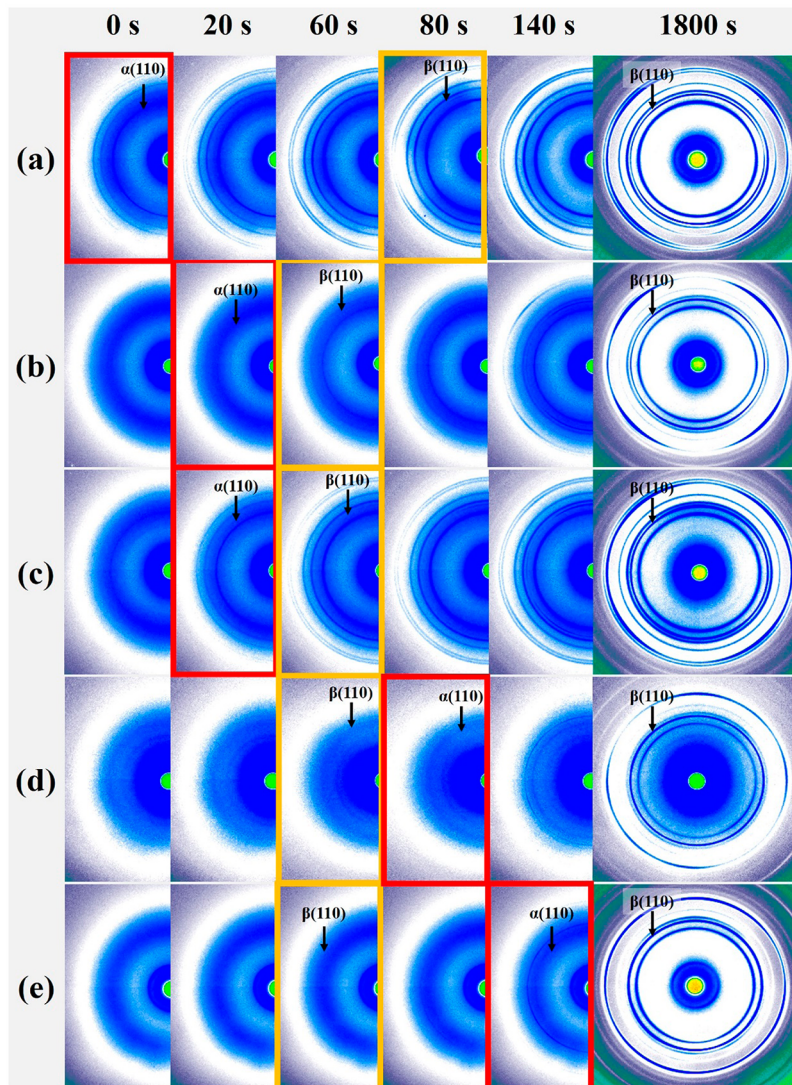


Figure 6. Selected 2D-WXAD patterns showing the crystal growth of iPP with 0.05 wt % β -NAs isothermally crystallized at 136 °C. (a) R0, (b) R5, (c) R15, (d) R30, and (e) Q. The shear direction is vertical. The red and yellow rectangles indicate the first appearance of α - and β -crystals, respectively.

oriented molecular chains to recover into the initial random coil state. In other words, shear-induced precursors that are metastable in nature tend to progressively dissolve into the amorphous matrix. This results in a precipitous decrease of the amount of α -nuclei. However, β -NA as the major cause of growth of β -crystals is not influenced by the shear (in terms of concentration). Therefore, β -crystals gradually become dominant as the relaxation time increases. A complete reversal happens when the relaxation time reaches 30 min, which is fairly analogous to the process undergone by the quiescently crystallized sample (Figure 7e).

To quantitatively study the influence of the relaxation time on the crystallization kinetics, the normalized relative crystallinity of all the samples as a function of isothermal crystallization time is displayed in Figure 8. By helping to overcome the crystal nucleation barrier,⁴⁷ shear flow is reported to be an efficient method to accelerate the crystallization process, which can also be promoted by β -NAs in terms of providing adequate nucleation sites.⁴⁵ Combining shear flow and β -NAs demonstrates a synergistic effect on the crystallization kinetics, as sample R0 exhibits the fastest

crystallization rate (Figure 8a) with the shortest half-crystallization time ($t_{0.5}$) (148.8 s, as shown in Table 1). As a matter of fact, a similar synergistic effect was also observed in the sheared iPP melt with CNTs or α -NAs as a consequence of the contribution of extra nuclei created by the interaction between the shear and fillers.^{24,48,49} Sample Q, where only β -NAs induced the quiescent crystallization (Figure 8e), yields the slowest crystallization process with the longest $t_{0.5}$ (425.0 s). The prolonged relaxation time gradually slows down the crystallization process (Figure 8, panels b–d); $t_{0.5}$ progressively extends (Table 1). The prolonged relaxation time means the accelerated effect of the shear flow field attenuates step-by-step as a result of the dissolution of oriented molecular chains at the high-relaxation temperature, leading to the incessant reduction of nucleation density. The reduction of nucleation density is also reflected by the delayed appearance of lamellar structures (Figure 2, panels b–d) and crystals (Figures 6 and 7, panels b–d). It is conceivable that the shear-enhanced crystallization kinetics will be completely “washed out” if the sheared melt is held at high temperatures for a sufficiently long relaxation time.

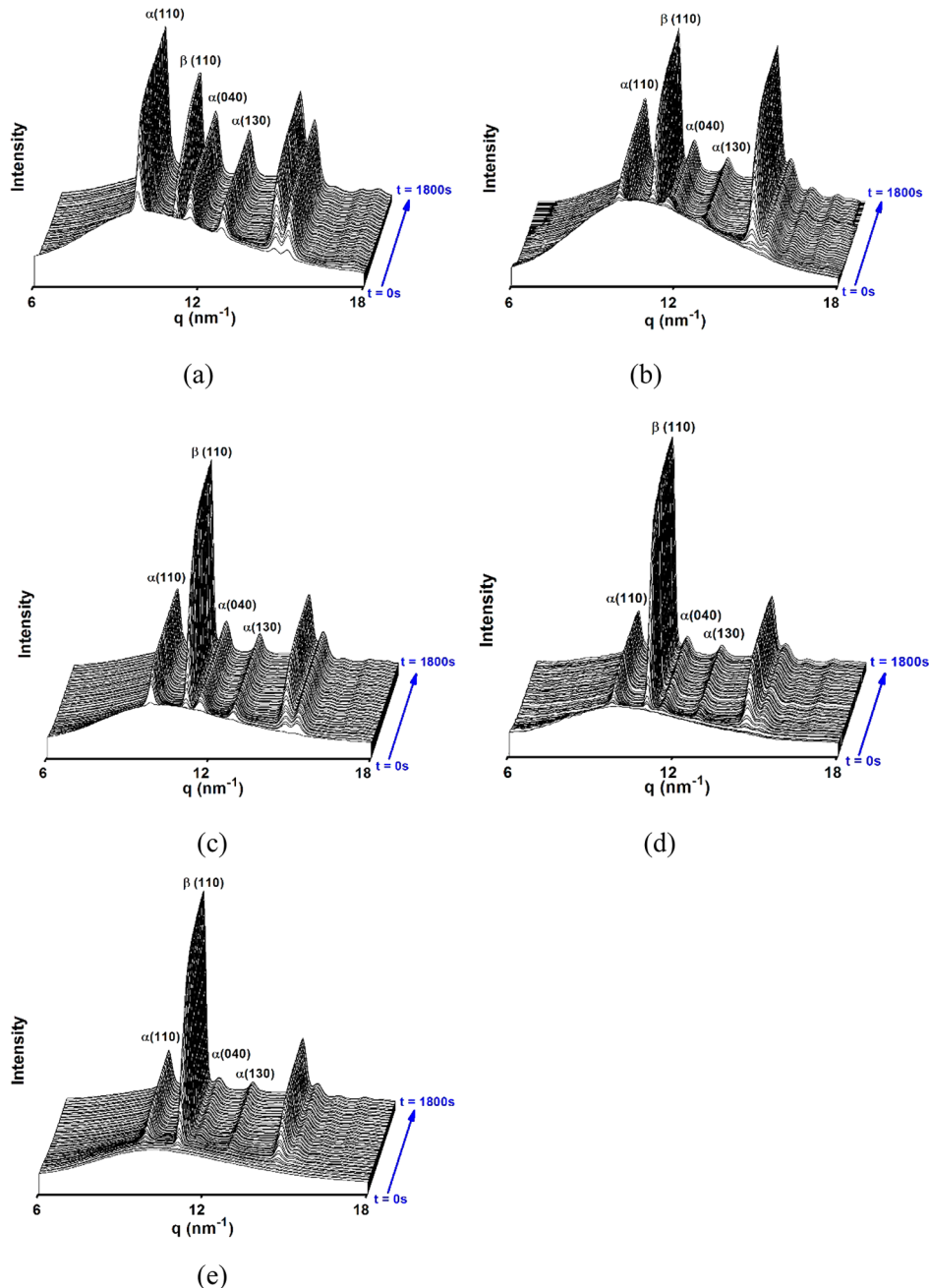


Figure 7. Linear WAXD intensity profiles as a function of the scattering sector (q) of iPP with 0.05 wt % β -NAs, obtained from circularly integrated intensities of 2D-WAXD patterns in Figure 6. (a) R0, (b) RS, (c) R15, (d) R30, and (e) Q.

The relaxation-controlled growth process of β -crystals is further revealed by the relative amount of β -crystals (K_β) and β -crystallinity (X_β) as a function of isothermal crystallization time, which are presented in Figures 9 and 10, respectively. As sample Q starts to isothermally crystallize, the very beginning K_β appears to be 100% (Figure 9e). This means the initial crystals are completely in the form of β -phase. The subsequent formation and growth of α -nuclei leads to a relative decline of β -crystals, and the final K_β levels off at 71% (Table 2). Accordingly, the final crystallinity of β -crystals in sample Q is the highest at approximately 35% (Table 2); meanwhile, the crystallization rate of β -crystals is the fastest (according to the slope of its curve in Figure 10e). Conversely, the development of β -crystals in sample R0 is strongly restricted by the application of shear flow in terms of nucleation and growth,

as manifested by the retarded appearance of β -crystals and the slowest crystallization rate (Figures 9a and 10a). Ultimately, sample R0 has the lowest β -crystals content compared to other samples ($K_\beta = 22\%$ and $X_\beta = 10\%$ in Table 2). Intermediate between samples Q and R0, the crystallization rate of β -crystals is accelerated, and its final content is enhanced with the increasing relaxation time (Figures 9 and 10, panels c–e). It is noted that the final K_β and X_β of sample R30 almost approach the values of sample Q. Further increasing the relaxation time will offer the opportunity for β -crystals to regain the maximum value, as in sample Q.

It was interesting to find that the overall crystallization kinetics were retained with increasing relaxation time, as opposed to the content variation of β -crystals. The former declined, whereas the latter increased. To extract the dynamic

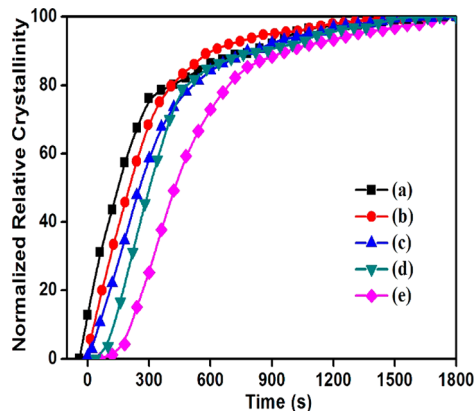


Figure 8. Normalized relative crystallinity as a function of isothermal crystallization time. (a) R0, (b) R5, (c) R15, (d) R30, and (e) Q.

Table 1. Half-Crystallization Time ($t_{0.5}$) and Avrami Exponent (n) of iPP with 0.05 wt % β -NAs when Isothermal Crystallization at 136 °C is Finished

samples	R0	R5	R15	R30	Q
$t_{0.5}$ (s)	148.8	201.8	251.6	301.9	425.0
n	0.8	1.0	1.3	2.4	3.8

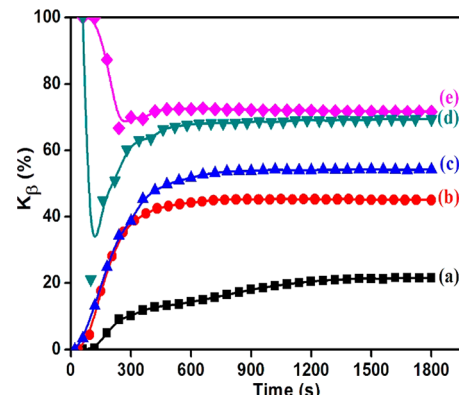


Figure 9. Relative amount of β -crystals (K_β) as a function of isothermal crystallization time. (a) R0, (b) R5, (c) R15, (d) R30, and (e) Q.

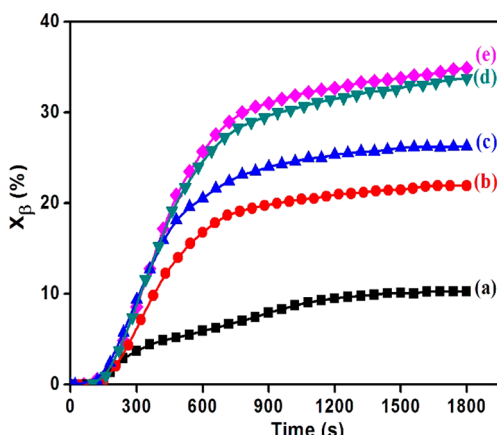


Figure 10. β -Phase crystallinity (X_β) as a function of isothermal crystallization time. (a) R0, (b) R5, (c) R15, (d) R30, and (e) Q.

Table 2. Final Relative Amount of β -Crystals (K_β) and β -Phase Crystallinity (X_β) of iPP with 0.05 wt % β -NAs when Isothermal Crystallization at 136 °C is Finished

samples	R0	R5	R15	R30	Q
K_β (%)	22	45	54	69	72
X_β (%)	10	22	26	34	35

quantitative relationship between these two opposite variations, two parameters are introduced here: relative shear efficiency (RSE) and relative recovery efficiency (RRE). Credit should be given to Alfonso et al., who developed the concept of RSE.⁵⁰ RSE is a quantity that is related to the residual effect of shear on the crystallization rate constant and is defined by the dimensionless number:

$$\text{RSE} = \frac{t_{0.5}(t_R) - t_{0.5}(Q)}{t_{0.5}(t_R = 0) - t_{0.5}(Q)} \quad (6)$$

where $t_{0.5}(t_R)$, $t_{0.5}(t_R = 0)$, and $t_{0.5}(Q)$ are the half-crystallization times of samples that have been relaxed for a time t_R , immediately quenched to T_c after the shear ($t_R = 0$) and quiescently crystallized (Q), respectively. RSE values must lie between 0 (no effect of flow on crystallization kinetics, in other words, quiescent crystallization) and 1 (maximum shear efficiency, when no relaxation step is interposed between the shear and the isothermal crystallization). RSE only reflects the relaxation phenomena leading to dissolution (or disappearance) of shear-induced nuclei and does not provide information on their overall concentration, which is obviously dictated by the imposed flow conditions, such as shear temperature, shear rate, and shearing time. Analogous to RSE, RRE is introduced by us to characterize the relative augment of β -crystals as a result of the decay of shear flow field.

$$\text{RRE} = \frac{K_\beta(t_R) - K_\beta(t_R = 0)}{K_\beta(Q) - K_\beta(t_R = 0)} \quad (7)$$

where $K_\beta(t_R)$, $K_\beta(t_R = 0)$, and $K_\beta(Q)$ are the final relative β -crystallinities of samples that have been relaxed for a time t_R for samples directly cooled to T_c after the shear ($t_R = 0$) and for the quiescent crystallization (Q), respectively. For the quiescent crystallization, RRE is equal to 1, indicative of the content of β -crystals at its maximum; when no relaxation step is interposed between the shear and the isothermal crystallization, RRE is equal to 0, where the content of β -crystals is at its minimum. RSE and RRE are then plotted against the isothermal crystallization time in Figure 11. A roughly linear decrease of RSE accompanying an approximately linear increase of RRE is observed with the increasing duration of the relaxation step. RSE is intimately associated with the unstable shear-induced oriented precursors developed in the molten polymers during the shearing step. The insertion of the relaxation step provides time for the progressive dissolution of shear-induced oriented precursors, such that the effect of the shear flow field attenuates. RSE reasonably decreases, while RRE dependent on β -NAs vibrantly rises. By extrapolating the straight line in Figure 11a to RSE = 0, the lifetime of shear-induced oriented precursors can be estimated, that is, 3244 s. This time, corresponding to the complete dissolution of the shear-induced oriented precursors (i.e., quiescent crystallization) is remarkably longer than the rheological relaxation time.⁵¹ Likewise, through extrapolating the straight line of RRE to 1, it is found that β -crystal content returning to its maximum (i.e., quiescent

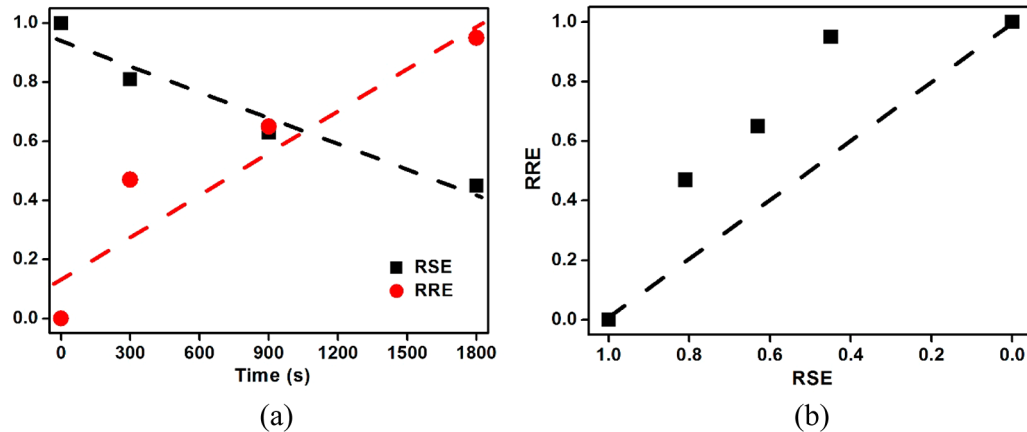


Figure 11. (a) Relative shear efficiency (RSE) and relative recover efficiency (RRE) as a function of time. (b) RRE as a function of RSE.

crystallization) only takes 1834 s, which is far shorter than the lifetime of shear-induced oriented precursors. This intriguing phenomenon illustrates that the attenuating rate of crystallization kinetics is fairly slower than the increasing rate of β -crystal content. In other words, the growth of β -crystals is not simply synchronous with, but also faster than, the dissolution of shear-induced oriented precursors. Straightforward evidence is further provided by the plot of RRE against RSE in Figure 11b. The only reasonable explanation for this result, we consider, is that the partially dissolved shear-induced oriented precursors as a result of relaxation have the ability to generate β -crystals instead of α -crystals upon the induction of β -NAs with the huge surface area. Only in this way can these precursors not only continue to accelerate the crystallization kinetics to some extent but also contribute to the formation of β -crystals. This intriguing finding enriches the formation mechanism of β -crystals, which is practically dependent on the β -nucleation sites given by β -NAs from a general point of view.²³

In addition to the crystallization kinetics, crystallization morphology is also greatly influenced by the relaxation process. Here, the Avrami equation is employed to reveal the nucleation mechanism and indirectly characterize the dimensionality of the total crystal growth, as shown below.

$$X(t) = 1 - \exp(-kt^n) \quad (4)$$

Equation 4 can be rewritten in the following form:

$$\log\{-\ln[1 - X(t)]\} = n\log(t) + \log(k) \quad (5)$$

where k is the bulk crystallization constant and n is the Avrami exponent. The normalized relative crystallinity $X(t)$ is derived from Figure 8. Corresponding Avrami plots are thus presented in Figure 12. A gradually ascending trend with the increasing relaxation time is manifested by the slope of the linear region of all the sheared samples (Figure 12, panels a–d); the largest slope appears in sample Q. The followed divergence in the late stage of crystallization is ascribed to the slow secondary crystallization, which usually happens after the fast primary crystallization.¹⁵ The Avrami exponent n is accordingly listed in Table 1. For the quiescent isothermal condition, n of sample Q is approximately 4.00, indicative of isotropic three-dimensional spherulitic growth of preformed nuclei originated from the thermal fluctuations and randomly distributed β -NAs in the iPP melt. Interestingly, n of sample R0 is almost equal to 1.00, roughly corresponding to one-dimensional crystal growth. This is consistent with previous SAXS patterns of sample R0, where

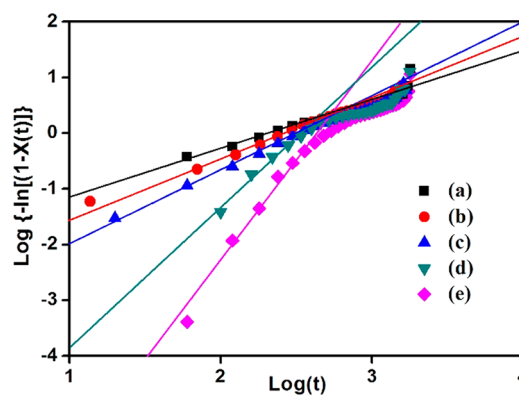


Figure 12. Avrami plots of the isothermal crystallization data at 136 °C of (a) R0, (b) R5, (c) R15, (d) R30, and (e) Q.

the growth of oriented α - and β -lamellae was observed. As the relaxation time increases, the residual samples (R5, R15, and R30) show a gradual rise of n toward the quiescent crystallization value. The longer relaxation time gives rise to the more severe dissolution of shear-induced oriented precursors and deviation of the needlelike β -NAs. Thus, the increase in random crystal growth and crystal growth dimensionality are reasonable.

To specifically emphasize the orientation of β -crystals affected by the relaxation process, the azimuthal diffraction of the $\beta(110)$ characteristic lattice plane is extracted and shown in Figure 13. According to the newly resolved orientation mode of β -crystals proposed by Yamaguchi et al.,¹⁹ six well-defined spots of the $\beta(110)$ lattice plane should be included in the WAXD patterns, of which two spots are present at the TD and four around $\pm 30^\circ$ off the MD. In our case, the β -crystal in sample R0 exhibits deficient orientation, as displayed by the irregular azimuthal diffraction of the $\beta(110)$ lattice plane, where only one sharp peak occurs at 210° (Figure 13a). The counteraction effect of the shear flow field and β -NAs deteriorates the formation of β -crystals, not only the content but also the orientation state. As the relaxation time increases to 15 min (R5 and R15), six diffraction peaks of the $\beta(110)$ lattice plane become more obvious (Figure 13, panels b and c), and illustrating the orientation of β -crystals is gradually refined. This is ascribed to the partial dissolution of shear-induced oriented precursors beneficial for the development of more β -crystals with more regular orientation. At the maximum relaxation time (30 min), the diffraction intensity of the $\beta(110)$ lattice plane is

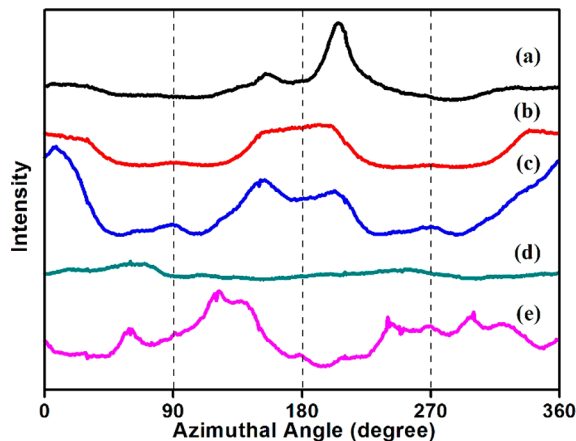


Figure 13. Azimuthal scan of the (110) lattice plane of β -crystals on the basis of Figure 6 when isothermal crystallization at 136 °C is finished. (a) R0, (b) R5, (c) R15, (d) R30, and (e) Q.

basically homogeneous without showing apparent diffraction peaks at the specific positions (Figure 13d). This relaxation time turns out to be long enough for the aligned needlelike β -NAs to return to the initial random state, inducing the growth of random β -crystals. These random β -crystals are even more homogeneous than the quiescently crystallized ones (Figure 13e). In this result, the appropriate relaxation time holds tremendous promise for realizing the “win-win” situation in terms of massive β -crystals with high orientation by regulating the state of shear-induced oriented precursors. In our case, relaxing β -nucleated iPP melt for 15 min at 170 °C after shear flow may be the optimal choice for obtaining many well-oriented β -crystals. Following the cessation of the shear flow, the relaxation process prior to crystallization is proved to be an effective intervention that helps to unify the seemingly contradictory factors (i.e., shear flow field and β -NAs) and take full advantage of their positive effects on the formation of oriented β -crystals. The shear flow field endows the needlelike β -NAs with a particular orientation, while oriented β -NAs induce the partially relaxed shear-induced oriented precursors to form the oriented β -crystals. The work carried out by Yamaguchi et al. is a source of examples demonstrating the successful formation of oriented β -crystals,^{19,20} even though they did not reveal the underlying mechanism.

To elaborately demonstrate the effect of relaxation of shear-induced oriented precursors on the formation of oriented β -crystals, a schematic diagram is depicted in Figure 14. Before the application of shear flow, the preformed needlelike β -NAs are randomly dispersed in the matrix of coiled iPP molecular chains. Upon the application of shear flow, both needlelike β -NAs and coiled iPP molecular chains tend to align along the shear flow direction. Shear-induced oriented precursors are successively generated in the iPP melt matrix and adjacent to the needlelike β -NAs. When being relaxed for a period of time at a high temperature, shear-induced oriented precursors start to dissolve, and those adjacent to the needlelike β -NAs are transformed into the oriented β -precursors due to the induction of β -NAs. Others in the matrix still maintain the ability to form oriented α -crystals. During the crystallization process, the oriented β -precursors form oriented β -crystals with their *c* axis perpendicular to the shear flow direction, while the residual shear-induced oriented precursors generate the oriented α -crystals whose *c* axis is parallel to the shear flow direction.

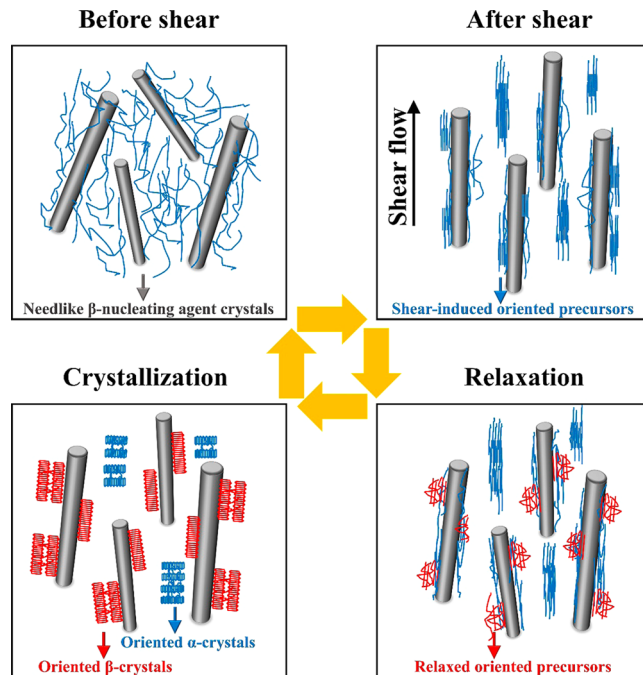


Figure 14. A schematic diagram of the effect of relaxation of oriented molecular chains on the formation of oriented β -crystals of iPP with β -NAs after shear flow. Red and blue lamellae correspond to oriented β - and α -lamellae, respectively.

Additional β -crystals may grow on the surface of oriented α -crystals due to the favorable isothermal crystallization temperature in this work.¹⁶

4. CONCLUSION

The effect of relaxation of shear-induced oriented molecular chains on the crystallization behavior of β -nucleated iPP was investigated by means of *in situ* synchrotron X-ray scattering. It was determined that as the increased relaxation time led to the enhanced dissolution of shear-induced oriented precursors, the content of β -crystals gradually tended to achieve its maximum obtained in the quiescent crystallization, while the entire crystallization process slowed to the state of quiescent crystallization. The predicted complete recovery time for β -crystal content (1834 s) was quite short compared to the lifetime of shear-induced oriented precursors (3244 s), which indicated that the partially dissolved shear-induced oriented precursors had the ability to induce β -crystals upon the absorption of needlelike β -NAs with huge surface area. Relaxation, introduced after shear flow but before crystallization, turned out to be an effective method to simultaneously preserve the content and refine the orientation of β -crystals in β -nucleated iPP, although the coexistence of shear flow and β -NAs is, in fact, unfavorable for β -crystals. In addition, the arrangement of oriented β -lamellae was first revealed by the unique cross SAXS patterns, where the *c* axis of oriented β -lamellae is perpendicular instead of parallel to the long-axis of needlelike β -NAs (shear flow direction) as a result of epitaxial growth.

ASSOCIATED CONTENT

S Supporting Information

The clarification of β -crystal lattice plane (Figure S1) and SAXS profiles (linear scale) of samples R5, R15, R30, and Q (Figure

S2). This material is available free of charge via the Internet at <http://pubs.acs.org>.

AUTHOR INFORMATION

Corresponding Author

*E-mail: zmli@scu.edu.cn. Tel: 86-28-85406866.

Notes

The authors declare no competing financial interest.

ACKNOWLEDGMENTS

The authors gratefully acknowledge the financial support of this work by the National Natural Science Foundation of China (Grants 51120135002, 51273114, 51227801, 51421061, and 51473135), the Innovation Team Program of Science & Technology Department of Sichuan Province (Grant 2014TD0002) and the Fundamental Research Funds for the Central Universities (Grant 3102014JCQ01096).

REFERENCES

- (1) Stocker, W.; Schumacher, M.; Graff, S.; Thierry, A.; Wittmann, J. C.; Lotz, B. Epitaxial Crystallization and AFM Investigation of a Frustrated Polymer Structure: Isotactic Poly(propylene), β Phase. *Macromolecules* **1998**, *31*, 807–814.
- (2) Karger-Kocsis, J.; Varga, J. Effects of Beta-Alpha Transformation on the Static and Dynamic Tensile Behavior of Isotactic Polypropylene. *J. Appl. Polym. Sci.* **1996**, *62*, 291–300.
- (3) Chen, H. B.; Karger-Kocsis, J.; Wu, J. S.; Varga, J. Fracture Toughness of Alpha- and Beta-Phase Polypropylene Homopolymers and Random- and Block-Copolymers. *Polymer* **2002**, *43*, 6505–6514.
- (4) Chen, Y. H.; Zhong, G. J.; Wang, Y.; Li, Z. M.; Li, L. B. Unusual Tuning of Mechanical Properties of Isotactic Polypropylene Using Counteraction of Shear Flow and beta-Nucleating Agent on beta-Form Nucleation. *Macromolecules* **2009**, *42*, 4343–4348.
- (5) Zhang, B.; Chen, J. B.; Cui, J.; Zhang, H.; Ji, F. F.; Zheng, G. Q.; Heck, B.; Reiter, G.; Shen, C. Y. Effect of Shear Stress on Crystallization of Isotactic Polypropylene from a Structured Melt. *Macromolecules* **2012**, *45*, 8933–8937.
- (6) Su, Z. Q.; Dong, M.; Guo, Z. X.; Yu, J. Study of Polystyrene and Acrylonitrile-Styrene Copolymer as Special Beta-Nucleating Agents to Induce the Crystallization of Isotactic Polypropylene. *Macromolecules* **2007**, *40*, 4217–4224.
- (7) Zhang, Z. S.; Wang, C. G.; Yang, Z. G.; Chen, C. Y.; Mai, K. C. Crystallization Behavior and Melting Characteristics of PP Nucleated by a Novel Supported Beta-Nucleating Agent. *Polymer* **2008**, *49*, 5137–5145.
- (8) Varga, J.; Menyhard, A. Effect of Solubility and Nucleating Duality of N,N'-Dicyclohexyl-2,6-Naphthalenedicarboxamide on the Supermolecular Structure of Isotactic Polypropylene. *Macromolecules* **2007**, *40*, 2422–2431.
- (9) Luo, F.; Geng, C. Z.; Wang, K.; Deng, H.; Chen, F.; Fu, Q.; Na, B. New Understanding in Tuning Toughness of beta-Polypropylene: The Role of Beta-Nucleated Crystalline Morphology. *Macromolecules* **2009**, *42*, 9325–9331.
- (10) Kalay, G.; Bevis, M. J. Processing and Physical Property Relationships in Injection Molded Isotactic Polypropylene 0.1. Mechanical Properties. *J. Polym. Sci., Part B: Polym. Phys.* **1997**, *35*, 241–263.
- (11) Kmetty, A.; Barany, T.; Karger-Kocsis, J. Self-Reinforced Polymeric Materials: A Review. *Prog. Polym. Sci.* **2010**, *35*, 1288–1310.
- (12) Li, J. X.; Cheung, W. L.; Chan, C. M. On Deformation Mechanisms of β -Polypropylene 2. Changes of Lamellar Structure Caused by Tensile Load. *Polymer* **1999**, *40*, 2089–2102.
- (13) Li, J. X.; Cheung, W. L.; Chan, C. M. On Deformation Mechanisms of β -Polypropylene 3. Lamella Structures after Necking and Cold Drawing. *Polymer* **1999**, *40*, 3641–3656.
- (14) Li, J. X.; Cheung, W. L. On the Deformation Mechanisms of β -Polypropylene: 1. Effect of Necking on β -Phase PP Crystals. *Polymer* **1998**, *39*, 6935–6940.
- (15) Chen, Y. H.; Mao, Y. M.; Li, Z. M.; Hsiao, B. S. Competitive Growth of α - and β -Crystals in β -Nucleated Isotactic Polypropylene under Shear Flow. *Macromolecules* **2010**, *43*, 6760–6771.
- (16) Varga, J.; Karger-Kocsis, J. Rules of Supermolecular Structure Formation in Sheared Isotactic Polypropylene Melts. *J. Polym. Sci., Part B: Polym. Phys.* **1996**, *34*, 657–670.
- (17) Li, H. H.; Jiang, S. D.; Wang, J. J.; Wang, D. J.; Yan, S. K. Optical Microscopic Study on the Morphologies of Isotactic Polypropylene Induced by Its Homogeneity Fibers. *Macromolecules* **2003**, *36*, 2802–2807.
- (18) Asano, T.; Furusho, T.; Alam, M. M.; Tamba, Y.; Sawatari, C.; Mina, M. F. Laser Light and X-Ray Diffraction Studies of Oriented Isotactic Polypropylene (iPP) Prepared by Temperature Slope Crystallization. *J. Macromol. Sci., Part B: Phys.* **2009**, *48*, 774–788.
- (19) Yamaguchi, M.; Fukui, T.; Okamoto, K.; Sasaki, S.; Uchiyama, Y.; Ueoka, C. Anomalous Molecular Orientation of Isotactic Polypropylene Sheet Containing N,N'-Dicyclohexyl-2,6-Naphthalenedicarboxamide. *Polymer* **2009**, *50*, 1497–1504.
- (20) Yamaguchi, M.; Irie, Y.; Phulkerd, P.; Hagihara, H.; Hirayama, S.; Sasaki, S. Plywood-Like Structure of Injection-Moulded Polypropylene. *Polymer* **2010**, *51*, 5983–5989.
- (21) Phulkerd, P.; Nobukawa, S.; Uchiyama, Y.; Yamaguchi, M. Anomalous Mechanical Anisotropy of Beta Form Polypropylene Sheet with N,N'-Dicyclohexyl-2,6-Naphthalenedicarboxamide. *Polymer* **2011**, *52*, 4867–4872.
- (22) Phulkerd, P.; Hagihara, H.; Nobukawa, S.; Uchiyama, Y.; Yamaguchi, M. Plastic Deformation Behavior of Polypropylene Sheet with Transversal Orientation. *J. Polym. Sci., Part B: Polym. Phys.* **2013**, *51*, 897–906.
- (23) Zhou, J. J.; Liu, J. G.; Yan, S. K.; Dong, J. Y.; Li, L.; Chan, C. M.; Schultz, J. M. Atomic Force Microscopy Study of the Lamellar Growth of Isotactic Polypropylene. *Polymer* **2005**, *46*, 4077–4087.
- (24) Chen, Y. H.; Zhong, G. J.; Lei, J.; Li, Z. M.; Hsiao, B. S. In Situ Synchrotron X-ray Scattering Study on Isotactic Polypropylene Crystallization under the Coexistence of Shear Flow and Carbon Nanotubes. *Macromolecules* **2011**, *44*, 8080–8092.
- (25) Somani, R. H.; Yang, L.; Zhu, L.; Hsiao, B. S. Flow-Induced Shish-Kebab Precursor Structures in Entangled Polymer Melts. *Polymer* **2005**, *46*, 8587–8623.
- (26) Turner-Jones, A.; Cobbold, A. J. The β Crystalline Form of Isotactic Polypropylene. *J. Polym. Sci., Part B: Polym. Lett.* **1968**, *6*, 539–546.
- (27) Mao, Y.; Li, X.; Burger, C.; Hsiao, B. S.; Tsou, A. H. 2D WAXS/SAXS Study on Isotactic Propylene-1-Butylene Random Copolymer Subjected to Uniaxial Stretching: the Influence of Temperature. *Polymer* **2013**, *54*, 1432–1439.
- (28) Mao, Y.; Li, X.; Burger, C.; Hsiao, B. S.; Mehta, A. K.; Tsou, A. H. Structure Development during Stretching and Heating of Isotactic Propylene-1-Butylene Random Copolymer: From Unit Cells to Lamellae. *Macromolecules* **2012**, *45*, 7061–7071.
- (29) Yang, H. R.; Lei, J.; Li, L.; Fu, Q.; Li, Z. M. Formation of Interlinked Shish-Kebabs in Injection-Molded Polyethylene under the Coexistence of Lightly Cross-Linked Chain Network and Oscillation Shear Flow. *Macromolecules* **2012**, *45*, 6600–6610.
- (30) Guinier, A.; Fournet, G. *Small-Angle Scattering of X-rays*; John Wiley: New York, 1955.
- (31) Tabatabaei, S. H.; Carreau, P. J.; Ajji, A. Effect of Processing on the Crystalline Orientation, Morphology, and Mechanical Properties of Polypropylene Cast Films and Microporous Membrane Formation. *Polymer* **2009**, *50*, 4228–4240.
- (32) Somani, R. H.; Hsiao, B. S.; Nogales, A.; Fruitwala, H.; Srinivas, S.; Tsou, A. H. Structure Development during Shear Flow Induced Crystallization of I-PP: In Situ Wide-Angle X-Ray Diffraction Study. *Macromolecules* **2001**, *34*, 5902–5909.
- (33) Somani, R. H.; Yang, L.; Hsiao, B. S.; Agarwal, P. K.; Fruitwala, H. A.; Tsou, A. H. Shear-Induced Precursor Structures in Isotactic

Polypropylene Melt by In-Situ Rheo-SAXS and Rheo-WAXD Studies. *Macromolecules* **2002**, *35*, 9096–9104.

(34) Soman, R. H.; Yang, L.; Hsiao, B. S. Precursors of Primary Nucleation Induced by Flow in Isotactic Polypropylene. *Phys. A* **2002**, *304*, 145–157.

(35) Hsiao, B. S.; Yang, L.; Soman, R. H.; Avila-Orta, C. A.; Zhu, L. Unexpected Shish-Kebab Structure in a Sheared Polyethylene Melt. *Phys. Rev. Lett.* **2005**, *94*.

(36) An, H. N.; Zhao, B. J.; Ma, Z.; Shao, C. G.; Wang, X.; Fang, Y. P.; Li, L. B.; Li, Z. M. Shear-Induced Conformational Ordering in the Melt of Isotactic Polypropylene. *Macromolecules* **2007**, *40*, 4740–4743.

(37) Balzano, L.; Rastogi, S.; Peters, G. W. M. Flow Induced Crystallization in Isotactic Polypropylene–1,3:2,4-Bis(3,4-Dimethylbenzylidene)Sorbitol Blends: Implications on Morphology of Shear and Phase Separation. *Macromolecules* **2008**, *41*, 399–408.

(38) Xu, J. Z.; Chen, C.; Wang, Y.; Tang, H.; Li, Z. M.; Hsiao, B. S. Graphene Nanosheets and Shear Flow Induced Crystallization in Isotactic Polypropylene Nanocomposites. *Macromolecules* **2011**, *44*, 2808–2818.

(39) Phillips, A. W.; Bhatia, A.; Zhu, P.-w.; Edward, G. Shish Formation and Relaxation in Sheared Isotactic Polypropylene Containing Nucleating Particles. *Macromolecules* **2011**, *44*, 3517–3528.

(40) Mao, Y. M.; Burger, C.; Zuo, F.; Hsiao, B. S.; Mehta, A.; Mitchell, C.; Tsou, A. H. Wide-Angle X-ray Scattering Study on Shear-Induced Crystallization of Propylene-1-Butylene Random Copolymer: Experiment and Diffraction Pattern Simulation. *Macromolecules* **2011**, *44*, 558–565.

(41) García-Gutiérrez, M. C.; Hernández, J. J.; Nogales, A.; Panine, P.; Rueda, D. R.; Ezquerra, T. A. Influence of Shear on the Tempered Crystallization of Poly(butylene terephthalate)/Single Wall Carbon Nanotube Nanocomposites. *Macromolecules* **2008**, *41*, 844–851.

(42) Hernández, J. J.; García-Gutiérrez, M. C.; Nogales, A.; Rueda, D. R.; Ezquerra, T. A. Shear Effect on Crystallizing Single Wall Carbon Nanotube/Poly(butylene terephthalate) Nanocomposites. *Macromolecules* **2009**, *42*, 4374–4376.

(43) Bruckner, S.; Meille, S. V.; Petraccone, V.; Pirozzi, B. Polymorphism in Isotactic Polypropylene. *Prog. Polym. Sci.* **1991**, *16*, 361–404.

(44) Vleeshouwers, S. Simultaneous In-Situ WAXS/SAXS and D.S.C. Study of the Recrystallization and Melting Behaviour of the α and β Form of IPP. *Polymer* **1997**, *38*, 3213–3221.

(45) Haeringen, D. T. V.; Varga, J.; Ehrenstein, G. W.; Vancso, G. J. Features of the Hedritic Morphology of β -Isotactic Polypropylene Studied by Atomic Force Microscopy. *J. Polym. Sci., Part B: Polym. Phys.* **2000**, *38*, 672–681.

(46) Luo, F.; Wang, K.; Ning, N.; Geng, C.; Deng, H.; Chen, F.; Fu, Q.; Qian, Y.; Zheng, D. Dependence of Mechanical Properties on β -Form Content and Crystalline Morphology for β -Nucleated Isotactic Polypropylene. *Polym. Adv. Technol.* **2011**, *22*, 2044–2054.

(47) Chan, N. Y.; Chen, M.; Hao, X. T.; Smith, T. A.; Dunstan, D. E. Polymer Compression in Shear Flow. *J. Phys. Chem. Lett.* **2010**, *1*, 1912–1916.

(48) Byelov, D.; Panine, P.; Remerie, K.; Biemond, E.; Alfonso, G. C.; de Jeu, W. H. Crystallization under Shear in Isotactic Polypropylene Containing Nucleators. *Polymer* **2008**, *49*, 3076–3083.

(49) Wang, J.; Yang, J.; Deng, L.; Fang, H.; Zhang, Y.; Wang, Z. More Dominant Shear Flow Effect Assisted by Added Carbon Nanotubes on Crystallization Kinetics of Isotactic Polypropylene in Nanocomposites. *ACS Appl. Mater. Interfaces* **2015**, *7*, 1364–1375.

(50) Cavallo, D.; Azzurri, F.; Balzano, L.; Funari, S. S.; Alfonso, G. C. Flow Memory and Stability of Shear-Induced Nucleation Precursors in Isotactic Polypropylene. *Macromolecules* **2010**, *43*, 9394–9400.

(51) Titomanlio, G.; Lamberti, G. Modeling Flow Induced Crystallization in Film Casting of Polypropylene. *Rheol. Acta* **2004**, *43*, 146–158.